Received February 2003
Revised June 2003
Accepted July 2003

Numerical studies of uniaxial powder compaction process by 3D DEM

Y. Sheng, C.J. Lawrence and B.J. Briscoe
Department of Chemical Engineering and Chemical Technology, Imperial College, London, UK

C. Thornton
Department of Civil Engineering, Aston University, Birmingham, UK

Keywords *Numerical analysis, Experimentation, Discrete manufacturing, Finite element analysis, Modelling, Simulation*

Abstract *In this paper, a 3D DEM program TRUBAL, which is capable of calculating the contact between particles considering friction and local plastic deformation, is employed to study the evolution of internal structure of particle assemblies during the consolidation process. Uniaxial powder compaction process is simulated in a cubic periodic unit cell by applying the strain rate to the individual particles. The selection of the proper time steps in DEM for quasi-static case is discussed. Results in particle scale (microscopic) are obtained and correlated to the statistical bulk response of the assembly. The effects of the microscopic properties of particles (such as friction, plastic contact) on the bulk mechanical response are examined by numerical tests. Correlations between the microscopic properties of particles and the macroscopic continuum behaviours of compacts are discussed. These discussions make it possible to fit DEM results at a macroscopic scale to the experimental measurements by adjusting the particle properties in DEM calculation. An example test is carried out to demonstrate that DEM results could be fitted properly to the experimental results, in the mean time, also provide some microscopic results which are hard to be measured. DEM has the potential to incorporate the microscopic properties of particles into a proper continuum model to perform combined macro and micro study of the powder compaction process.*

1. Introduction

Powder compaction is widely used in the pharmaceutical, ceramic and automotive industries to produce near net shape components with complex geometry and high strength. Compaction induces very complex states of stress in the powder compact which sometimes cause processing problems in industry, such as "capping" which is often encountered in pharmaceutical tabletting process. Many experimental and theoretical studies based on continuum mechanics have been carried out to study the macroscopic mechanical responses of compacts, and many constitutive laws for powder forming processes have been proposed (Adams and Briscoe, 1994;

Engineering Computations
Vol. 21 No. 2/3/4, 2004
pp. 304-317

0264-4401
DOI 10.1108/02644400410519802

The work in this paper is supported by the Engineering and Physical Sciences Research Council (EPSRC) in the UK, through grant number GR/N13050.

Aydin *et al.*, 1995; Briscoe and Evans, 1991; MacLeod and Marshall, 1977; Satake, 1982; Train, 1957; Walker, 1966; Yousuff and Page, 1993). In recent years, the finite element method (FEM) has also been adopted in simulations of powder compaction (Aydin *et al.*, 1996; Briscoe and Rough, 1998; Coube and Riebel, 2000; Sheng *et al.*, 2001; Zahlan *et al.*, 2001). Although continuum methods (including FEM) are effective in studying the macroscopic densification process in compaction, it should be noted that the accuracy of the results strongly depends upon the constitutive model and the quality of the material parameters (Adams and Briscoe, 1994; Briscoe and Evans, 1991; Satake, 1982; Walker, 1966; Yousuff and Page, 1993). Furthermore, in continuum models, the microscopic properties of particles and the interactions between particles, which strongly influence the macroscopic behaviour, cannot be considered. To obtain optimal mechanical properties of green compacts, better knowledge of the relation between powder characteristics and mechanical behaviour of the material during compaction is required.

The discrete element method, developed by Cundall and Strack (1979), is an effective numerical tool to investigate the micro mechanics of granular materials (Gethin *et al.*, 2001; Martin *et al.*, 2003; Redanz and Fleck, 2001; Thornton and Antony, 2000; Thornton and Sun, 1993). In DEM, each individual particle of an assembly is modelled separately and its motion is defined from the interactions with neighbouring particles. The detailed movements of particles can be traced. As a consequence, microscopic evolution of the internal stress and the structure of the assembly can be obtained. In the mean time, the macro behaviour of the whole assembly can be obtained by statistical means.

In this paper, a 3D DEM code TRUBAL (Thornton, 1996; Thornton and Antony, 2000; Thornton and Sun, 1993; Thornton and Yin, 1991), which is capable of modelling friction, cohesion and local plastic deformation at the inter-particle contacts, is used to simulate quasi-static uniaxial compaction of various kinds of powder materials. First, the critical time step that is proper for quasi-static simulation is discussed by compressing a glass ballotini assembly. The evolution of internal structure of the particle assembly, such as coordination number and plastic contact number, is investigated along with correlated statistical macroscopic behaviours such as stress-strain relations and anisotropy of the compacts. The link between particle interactions and mechanical properties of the compacts is thereby identified through the DEM results. Finally, an experiment of die compaction of alumina powder is carried out; bulk mechanical responses of the compact are measured and compared to the equivalent DEM calculation with adjustable material properties of the particles. When the macroscopic DEM results agree with experimental ones, the calculation can also reveal evolution of internal structure of particle assembly during the compaction which is very difficult to be measured in experiment. Thus, the work in this paper shows the potential of DEM to incorporate the microscopic properties of particles into a proper continuum

model to perform combined macro and micro study of the powder compaction process.

2. Discrete element model for quasi-static simulations

The DEM is a time dependent finite difference scheme. The progressive movement of each constituent particle and incremental contact forces are cyclically calculated by Newton's second law of motion, according to which, the equations of motion of a particle over a time step Δt are given as follows (Cundall and Strack, 1979)

Translation

$$F_i - \beta_g v_i = m\frac{\Delta v_i}{\Delta t} \tag{1}$$

Rotation

$$M_i - \beta_g \omega_i = I\frac{\Delta \omega_i}{\Delta t} \tag{2}$$

where $i = 1, 2, 3$ indicates the three components in x-, y-, z- directions, F_i is the out of balance force component of the particle, v_i is the translational velocity, m is the mass of the particle, M_i is the out of balance moment due to contacts, ω_i is the rotational velocity, I is the rotational inertia of the particle, β_g is the global damping coefficient and t is time.

Equations (1) and (2) are solved with a finite difference scheme to give the velocity increments of each particle. The updated velocities of each particle are used to find the relative approach between contacting particles. After sorting the contacts, the incremental contact forces can be calculated according to a prescribed contact-displacement law. The contact forces are resolved to obtain out of balance forces on each particle, from which new accelerations of each particle are then calculated at the next time step.

For a quasi-static problem, such as the powder compaction process, the load is applied very slowly, and entire loading and unloading process can last several hours. The acceleration of the particles on right hand side of Equation (1) will be very small. If the time step is not chosen properly in this case, it will cause problems with convergence of the calculations, or the calculation steps will become enormous and exceed the capacity of the computer.

In the current version of TRUBAL (Thornton and Antony, 2000), the time step is based on the consideration of the Rayleigh wave speed of force transmission around the surface of elastic bodies. Upon an application of a force to an elastic body, Rayleigh waves propagate along the surface with a velocity

$$v_R = \alpha\sqrt{\frac{G}{\rho}} \tag{3}$$

where ρ is the density of the material, G is the shear modulus and α is the root of following equation,

$$(2-\alpha^2)^4 = 16(1-\alpha^2)\left[1-\frac{1-2\nu}{2(1-\nu)}\alpha^2\right] \tag{4}$$

from which an approximation can be made as,

$$\alpha = 0.1631\nu + 0.876605 \tag{5}$$

in which ν is Poisson's ratio for the material.

For an assembly of many spherical particles, it can be shown that the highest frequency of Rayleigh wave propagation is determined by the smallest spheres, and gives the critical time step as,

$$\Delta t = \frac{\pi R_{\min}}{v_R} = \frac{\pi R_{\min}}{\alpha}\sqrt{\frac{\rho}{G}} \tag{6}$$

As an example, to demonstrate the effect of the time step, if all the particles are given the following properties: Young's modulus 70 MPa, Poisson's ratio 0.3, notional solid density 2,650 kg/m^3, diameter 10 μm, the time step would be ca. 1 μs according to equation (6). In order to ensure a quasi-static deformation of the particle assembly, the strain rate applied should not be more than $10^{-5}\,s^{-1}$, it would require 10^{10} time steps to apply 10 per cent strain to the assembly. To complete the simulations within a reasonable time, a density scaling method has been used to increase the magnitude of the time step. As a consequence, there will be order of magnitude changes of the velocities and accelerations of the particles. However, the contact forces and displacement of particles will also be affected if the density scale is not properly selected.

Figure 1 shows the results of the assessment of the density scaling with different combinations of strain rates and notional densities. A dimensionless variable is defined as

$$\left[\frac{\dot{\varepsilon}^2\rho R_{\min}^2}{p_y}\right]^{1/2}$$

to consider the effect of the density scales for various strain rates applied to the particle assembly, where $\dot{\varepsilon}$ is the strain rate applied to the particle assembly, ρ is the density of the particles, $R_{\min}$ is the diameter of the smallest particle, and p_y is the limiting contact pressure between the particles.

Apparently, there is a transition zone, in which the axial stress at 10 per cent strain changes dramatically with the strain rate and density. The upper level line indicates the dynamic response of the assembly caused by rising magnitude of the strain rate or density beyond a certain level. The results on the lower level line are considered to reflect the stable static response of the assembly. Between these two horizontal lines, the results for the stress depend on the density scaling. Therefore, the notional density should be carefully

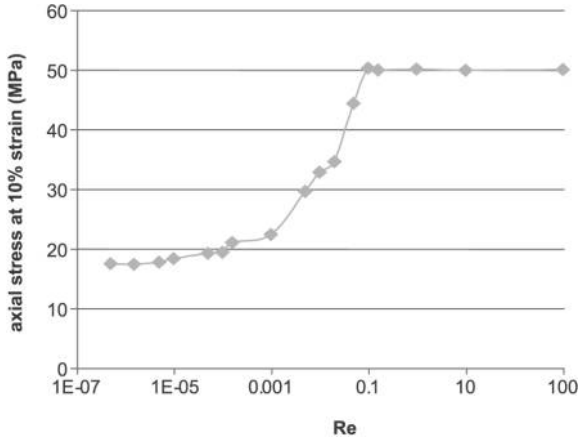

Figure 1.
Density scaling of the quasi-static problems

selected to guarantee that the results are within the quasi-static region. For the strain rate of $10^{-5}\,s^{-1}$, the notional density can be scaled up by a factor of 10^{12} according to these calculations. All the results presented in this paper have the scaling factor chosen within the quasi-static zone.

The DEM programme used in this paper models the particles as elastic spheres with inter-particle friction and cohesion. A plastic contact algorithm is used which assumes the normal contact pressure initially to have an elastic Hertzian distribution, then after a limiting contact pressure p_y, to have a truncated Hertzian distribution (Thornton, 1996; Thornton and Yin, 1991). Simulations are carried out in a representative volume element (unit cell) with periodic boundaries. This method eliminates the influence of the boundary conditions in compaction, thus represents an idealized model. To study the correlations between particle properties and bulk behaviour of compacts, spherical particles are randomly packed in a cubic cell of dimension 0.3 mm. The properties of the particles and other parameters in the simulation are listed in Table I.

First, the assembly is isotropically compressed until an isotropic stress of 100 kPa is reached to set up the initial contacts between particles using the following servo-control algorithm,

$$\dot{\varepsilon}_1 = \dot{\varepsilon}_2 = \dot{\varepsilon}_3 = g(p_d - p_c) \tag{7}$$

Dimension of unit cell	$0.3 \times 0.3 \times 0.3$ mm
Diameter of particles	136-280 μm
Mean diameter of particles	200 μm
Number of particles in unit cell	1,000
Young's modulus of particles	70 MPa
Poisson's ratio of particles	0.3
Friction coefficient	0.3-0.9
Limiting contact pressure	0.5 and 1.0 GPa

Table I.
Parameters used in numerical tests

where p_d is the desired isotropic stress and p_c is the calculated isotropic stress. An initial strain rate should be specified, which is progressively modified using a value for the gain parameter g calculated from

$$g = \left(\frac{\dot{\varepsilon}}{p_d - p_c} \right)_{\text{initial}} \tag{8}$$

This method is also used to apply the uniaxial compaction by fixing the particle movement in the first and third directions and just applying the strain rate to second direction until the desired axial stress is obtained.

3. Relation between particle properties and bulk response of the compacts

Numerical tests have been carried out to study the correlations between the material properties of particles and the mechanical response of the compact. Parameters used in the calculations are listed in Table I. Both loading and unloading in the compaction process of the particle assembly have been simulated in DEM tests. The stress-strain curves obtained by statistical means from four DEM calculations with different inter-particle friction coefficients are shown in Figure 2. As the friction coefficient is reduced from 0.9 to 0.3, for the same stress applied, the strain (deformation) of the compact is larger for smaller inter-particle friction. Or for the same strain value, the stress values for cases with larger inter-particle friction are higher than for smaller friction. Higher inter-particle friction prevents the particles from free movement and sliding and thus makes the whole assembly stiffer. The unloading curves in Figure 2 show elastic recovery in most of the unloading process and a small portion of inelastic deformation at the end of unloading. This phenomenon has also been observed in experiments (Adams and Briscoe, 1994; Briscoe and Rough, 1998; Satake, 1982). After unloading, the final plastic deformations of

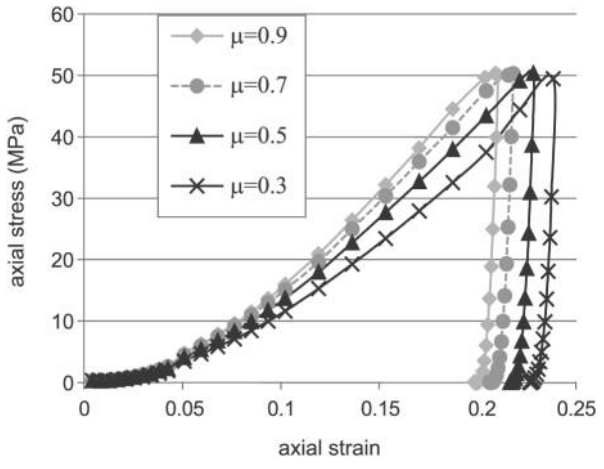

Figure 2.
Stress-strain curves for different friction coefficients

the compacts also increase with the decrease of the inter-particle friction. These are rational trends of the stress-strain relation considering the effect of inter-particle friction. Figure 3 depicts the variation of the axial stress and the lateral stress in the same set of numerical tests as in Figure 2. When the same axial stress is applied to the assembly, the smaller inter-particle friction cases have larger lateral stress. In the smaller friction case, it is easier to move and re-arrange the particles, finally giving an internal structure that can transmit the forces between particles more efficiently; this could also be considered as a decrease of the anisotropy of the compacts.

The DEM programme used in this work is capable of simulating plastic contacts between the particles. Numerical tests have also been carried out to study the effect of plastic contacts on the macroscopic properties of the assembly. As shown in Figure 4, when the assembly is subjected to the same axial stress, the strain of the assembly increases from the result for $p_y = 1\,\text{GPa}$ to the result for $p_y = 0.5\,\text{GPa}$, where P_y is the limit contact pressure. The lower the limiting contact pressure assumed, the softer is the particle assembly. Figure 5 shows the effect of the limiting contact pressure on the relationship between axial and lateral stress. When the limiting contact pressure is reduced, the softening of the assembly leads to greater strains and increased anisotropy; the lateral stress is therefore reduced.

Figures 6 and 7 show the effect of the particle properties on the internal structure of the assembly. First, the variations of the coordination number are shown. The average coordination number is usually defined as:

$$Z = 2C/N \tag{9}$$

where C is the number of contacts and N is the number of particles.

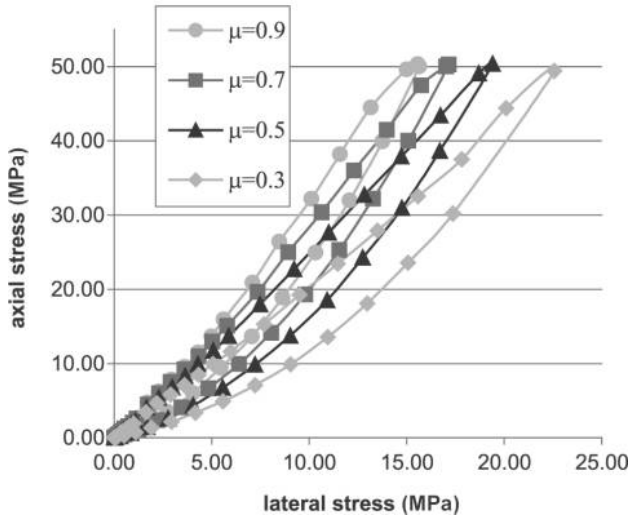

Figure 3.
Effect of the friction coefficient on the axial stress-lateral stress curves

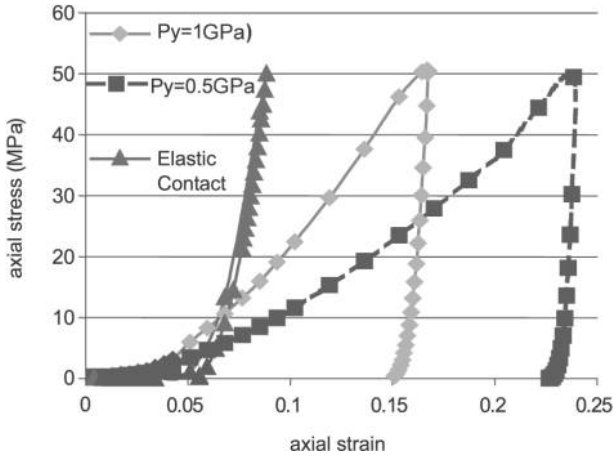

Figure 4.
Stress-strain curves for different limiting contact pressure

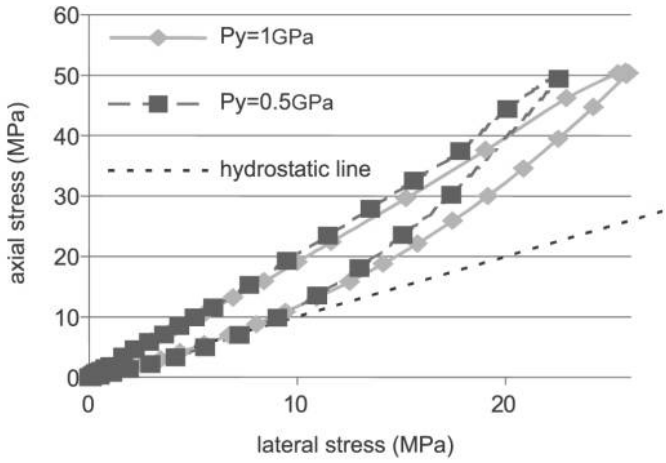

Figure 5.
Effect of limiting contact pressure on the axial stress-lateral stress curves

However, in the compaction tests, there are some particles with no contacts or one contact. None of these particles contribute to the state of stress. Therefore, a mechanical average coordination number is defined as (Thornton and Antony, 2000; Thornton and Sun, 1993)

$$Z_{\mathrm{m}} = \frac{(2C - N_1)}{(N - N_0 - N_1)} \tag{10}$$

where N_0 and N_1 are the number of particles with no and one contact, respectively. In Figure 6, decreasing the inter-particle friction increases the coordination number. Particles are easier to move in low friction cases, thus allowing more contacts to be set up. Reducing the limiting contact pressure also

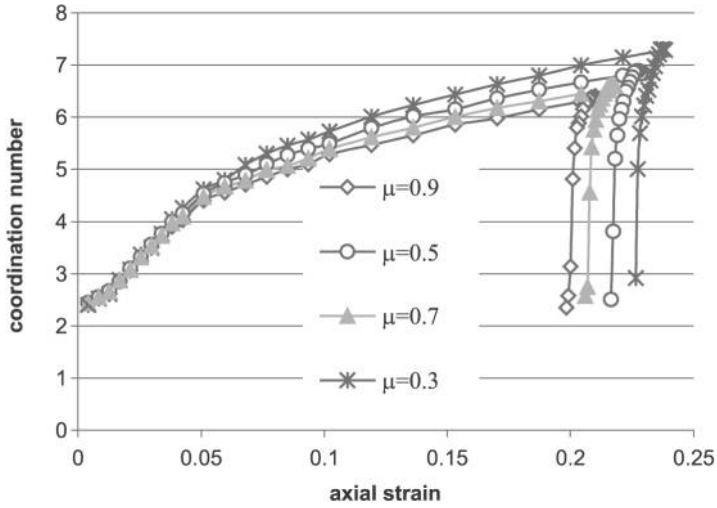

Figure 6.
Evolution of the coordination number with different inter-particle friction

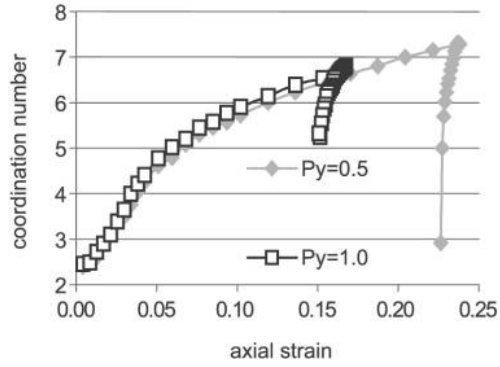

Figure 7.
Evolution of the coordination number with different limiting contact pressure

produces a small increase in the coordination number (Figure 7). This is principally due to the increased strain.

The plastic contact numbers have been calculated in all above numerical tests and are shown in Figures 8 and 9. Comparing Figure 8 with Figure 2, the plastic contact number increases during the loading period, and has a slight drop upon unloading (Figure 8). The remaining plastic contacts form the major part of the unrecoverable plastic deformation of the assembly (Figure 2). When reducing the friction between the particles, the maximum and final (after unloading) plastic contact numbers increase. This means that more plastic contacts occur in cases with smaller inter-particle friction, when the assembly is compressed to the same strain. The coordination numbers and the bulk plastic deformation of assemblies of particles with smaller inter-particle friction also increase with the plastic contact numbers. These phenomena are

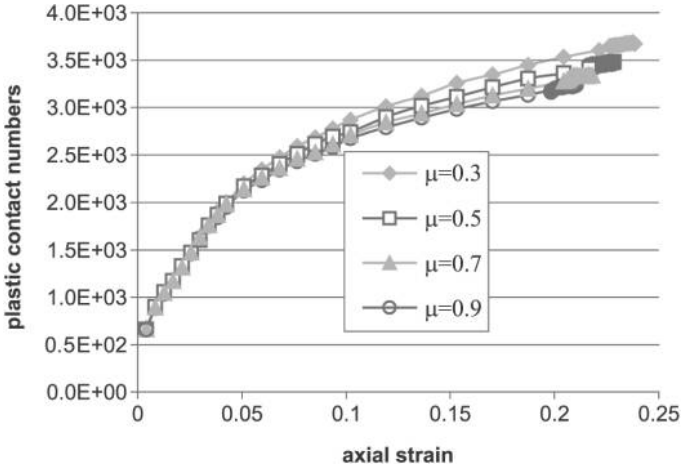

Figure 8.
Evolution of the plastic contact number with different inter-particle friction

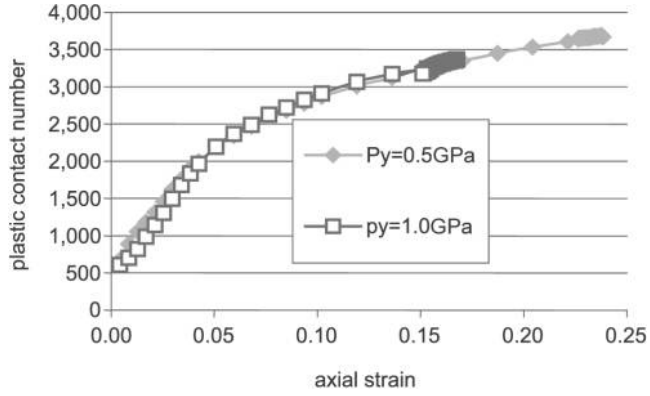

Figure 9.
Evolution of the plastic contact number with different limiting contact pressure

correlated with each other and reflect the fact that the changes of the particle properties and microscopic structures of the particle assembly have appreciable effects on the bulk mechanical response of the compacts. Similar relations between internal microstructure and bulk behaviour can also be found by comparing Figure 9 with Figures 4 and 7. An increase of the limiting contact pressure reduces the number of plastic contacts (Figure 9) and thus reduces the coordination number (Figure 7) and the bulk plastic deformation of the compacts (Figure 4).

4. An uniaxial powder compaction test

An experiment of powder compaction is carried out to compare with and validate the DEM calculations. Alumina powder (α-Al_2O_3, AKP-30, Sumitomo Chemical Co., Ltd) is used to form the agglomerates incorporated with a

commercial grade poly (vinyl alcohol) PVA binder (BDH chemicals Ltd). The mean size of the agglomerates was controlled around 600 μm by conventional sieving method. Then, the alumina agglomerates are poured into a square hardened steel die, in dimension of $1.2 \times 1.2 \times 0.7$ cm, and single-side pressed in a universal testing machine (Model T100, Instron) with a crosshead speed of 5 mm/min. Attached transducers record the pressure and the movement of the top punch. The loading-unloading curve (average compaction pressure against voids ratio in the compact), and the compaction curve (average density against compaction pressure) obtained in experiments are plotted in Figures 10 and 11. The average density of compact is derived from the volumetric strain in both experiments and DEM calculations as follows.

$$\rho = \rho_0 \exp[-\varepsilon_v] \tag{11}$$

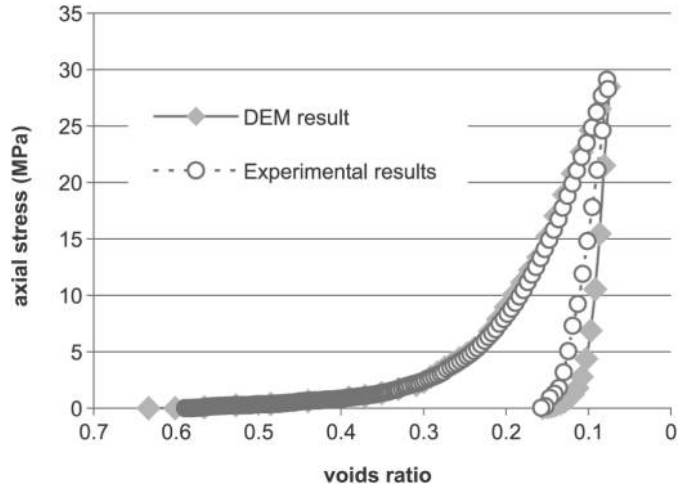

Figure 10.
Loading-unloading curve of the square die compaction tests

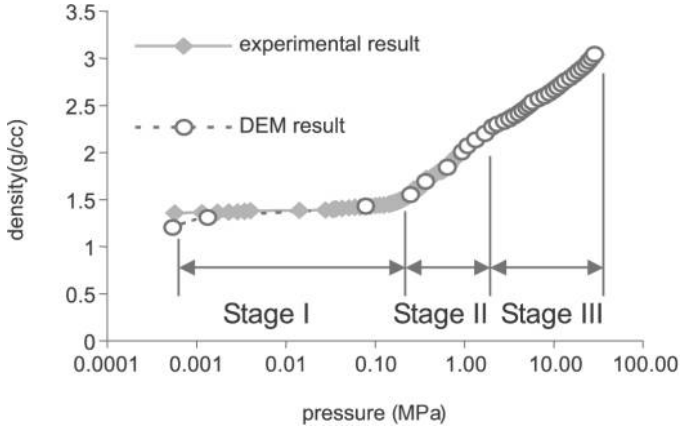

Figure 11.
Compaction curve of the square die compaction tests

in which $\varepsilon_v = \varepsilon_Z + \varepsilon_Y + \varepsilon_X$ is the volumetric strain, ρ_0 is the initial tapping density before compaction.

DEM calculation is also carried out with same conditions of experiment apart from the inter-particle friction and the limit contact pressure, which are adjusted during the loading and unloading process to make sure that the bulk response of the compact agree with the measurement. The properties used in the DEM calculation are listed in Table II. The DEM results of loading-unloading curve, and compaction curve are also plotted in Figures 10 and 11 to compare with experimental ones.

From the figures, DEM results of the bulk response of the compact can be fitted properly to the experimental results, especially in compaction curves, both curves clearly show the different stages in the powder compaction. In Figure 11, stage I refers to the particle rearrangement process, particles are filling the voids in the assembly, and set up the contacts with the adjacent particles, thus can barely take on the load. Stage II is the initial compaction period, and most of the elastic deformation happen, and plastic deformation at some contacts of particles also starts. In stage III, most of particles have settled and plastic deformations at the contact occur in a very high ratio, compact is very hard to achieve further densification; even compaction pressure is very high. Apart from the macro scale results which are fitted to the experimental results, DEM calculation can also provide the results in micro scale, the evolution of coordination numbers of the compact is shown in Figure 12. The coordination number increases with the compaction load, and the speed of

Dimension of unit cell	$12 \times 12 \times 7$ mm
Diameter of particles	450-650 μm
Mean diameter of particles	600 μm
Number of particles in unit cell	3,200
Young's modulus of particles	3.5 GPa
Poisson's ratio of particles	0.3
Friction coefficient	0.3-0.5
Limiting contact pressure	20-200 MPa

Table II.
Properties used in square die compaction

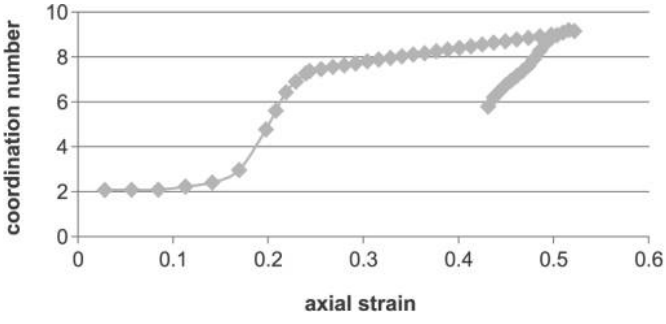

Figure 12.
Evolution of internal structure by DEM in square die compaction test

increase varies during different compaction stages corresponding to Figure 11. In particle rearrangement stage, many particles are free to move, few contacts can be set up, and so coordination number is low. When particles fill all the voids and contacts begin to set up, coordination number increases very fast in stage II. After most particles settle down and more plastic deformation appear at the contact, coordination number reaches a stable level, and increases very slow with the pressure. Thus, the macro behaviour of the compact and evolution of internal structure in micro level can be correlated with each other by DEM simulations.

5. Conclusion

Based on 3D DEM simulations of the powder compaction process, detailed information about the evolution of the micro level internal structure of particle assemblies has been obtained and compared with the correlated bulk mechanical response of the compacts. Relationships between the particle properties, microstructures of the assembly and the macro behaviour of the compacts have been determined and discussed. Several rational trends of these relationships have been demonstrated using the DEM results. Although some of the particle properties are not assigned practical values, they are carefully chosen to show the great influence they can have on the mechanical properties of green compacts in the compaction process. A comparison of experimental and DEM results on a square die compaction test has demonstrated the potential of DEM simulations to consider micro level particle properties in the analysis of the bulk mechanical response of compact. Specific material properties of the particles will be introduced into the simulations to quantify the relationship between the microstructure and macro behaviour of the compacts in the further research.

References

Adams, M.J. and Briscoe, B.J. (1994), "Deterministic micromechanical modelling of failure or flow in discrete planes of densely packed particle assembles: introductory principles", in Metha, A. (Ed.), *Granular Matter*, Springer-Verlag, New York, NY, p. 259.

Aydin, I., Briscoe, B.J. and Özkan, N. (1995), "3-D profiles and surface topography of alumina compacts", *Int. J. Machine Tools and Manufacture*, Vol. 35, pp. 345-52.

Aydin, I., Briscoe, B. and Sanliturk, K.Y. (1996), "The internal form of compacted ceramic components: a comparison of finite element modelling with experiments", *Powder Technology*, Vol. 89, pp. 239-54.

Briscoe, B.J. and Evans, P.D. (1991), "Wall friction in compaction of agglomerated ceramic powder", *Powder Technology*, Vol. 65, pp. 7-20.

Briscoe, B.J. and Rough, S.L. (1998), "The effects of wall friction in powder compaction", *Colloids and Surfaces A*, Vol. 137, pp. 103-16.

Coube, O. and Riebel, H. (2000), "Numerical simulation of metal powder die compaction with special consideration of cracking", *Powder Metallurgy*, Vol. 43 No. 2, pp. 123-31.

Cundall, P.A. and Strack, O.D.L. (1979), "A discrete numerical model for granular assemblies", *Géotechnique*, Vol. 29, pp. 47-65.

Gethin, D.T., Ransing, R.S., Lewis, R.W., Dutko, M. and Crook, A.J.L. (2001), "Numerical comparison of a deformable discrete element model and an equivalent continuum analysis for the compaction of ductile porous material", *Computers and Structures*, Vol. 79 No. 13, pp. 1287-94.

MacLeod, H.M. and Marshall, K. (1977), "The determination of density distribution in ceramic compacts using autoradiography", *Powder Technology*, Vol. 16, p. 107.

Martin, C.L., Bouvard, D. and Shima, S. (2003), "Study of particle rearrangement during powder compaction by the discrete element method", *J. Mech. and Phys. Solids*, Vol. 51 No. 4, pp. 667-93.

Redanz, P. and Fleck, N.A. (2001), "The compaction of a random distribution of metal cylinders by the discrete element method", *Acta Materialia*, Vol. 49 No. 20, pp. 4325-35.

Satake, M. (1982), *Deformation and Failure of Granular Materials*, in Vermeer, P.A. and Luger, H.J. (Eds), Balkema, Rotterdam, pp. 63-8.

Sheng, Y., Lawrence, C.J. and Briscoe, B.J. (2001), "An explanation of internal density gradients during the entire compaction cycle of powders", in Adair, J.H., Puri, V.M. and Haris, K.S. (Eds), *Fine Powder Processing*, pp. 207-13.

Thornton, C. (1996), "From contact mechanics to particulate mechanics", in Adams, M.J., Biswas, S.K. and Briscoe, B.J. (Eds), *Solid-Solid Interactions*, Imperial College Press, pp. 250-64.

Thornton, C. and Antony, S.J. (2000), "Quasi-static shear deformation of a soft particle system", *Powder Technology*, Vol. 109, pp. 179-91.

Thornton, C. and Sun, G. (1993), "Uniaxial compression of granular media: numerical simulation and physical experiment", in Thornton, C. (Ed.), *Powders and Grains*, Vol. 93, Balkema, Rotterdam, pp. 129-34.

Thornton, C. and Yin, K.K. (1991), "Impact of elastic spheres with and without adhesion", *Powder Technology*, Vol. 65, pp. 153-66.

Train, D. (1957), "Transmission of forces through a powder mass during the process of pelleting", *Trans. Inst. Chem. Eng.*, Vol. 35, p. 258.

Walker, D.M. (1966), "An approximate theory for pressure and arching in hoppers", *Chem. Eng. Sci.*, Vol. 21, pp. 975-97.

Yousuff, M. and Page, N.W. (1993), "Die stress and internal friction during quasi-static and dynamic powder compaction", *Powder Technology*, Vol. 76, pp. 299-307.

Zahlan, N., Knight, D.T., Backhouse, A. and Leiper, G.A. (2001), "Modelling powder compaction and pressure cycling", *Powder Technology*, Vol. 114, pp. 112-7.

This article has been cited by:

1. Dongwoo Sohn, Youngmin Lee, Mu-Young Ahn, Yi-Hyun Park, Seungyon Cho. 2018. Numerical prediction of packing behavior and thermal conductivity of pebble beds according to pebble size distributions and friction coefficients. *Fusion Engineering and Design* **137**, 182-190. [Crossref]
2. Bereket Yohannes, Xue Liu, Gary Yacobian, Alberto M. Cuitiño. 2018. Particle size induced heterogeneity in compacted powders: Effect of large particles. *Advanced Powder Technology* **29**:12, 2978-2986. [Crossref]
3. Lei Zhang, T. Matthew Evans. 2018. Boundary effects in discrete element method modeling of undrained cyclic triaxial and simple shear element tests. *Granular Matter* **20**:4. . [Crossref]
4. Y.T. Feng, Tingting Zhao, Min Wang, D.R.J. Owen. 2018. Characterising particle packings by principal component analysis. *Computer Methods in Applied Mechanics and Engineering* **340**, 70-89. [Crossref]
5. Omid Dorostkar, Jan Carmeliet. 2018. Potential Energy as Metric for Understanding Stick–Slip Dynamics in Sheared Granular Fault Gouge: A Coupled CFD–DEM Study. *Rock Mechanics and Rock Engineering* **51**:10, 3281-3294. [Crossref]
6. Yi He, Feihong Guo. 2018. Micromechanical analysis on the compaction of tetrahedral particles. *Chemical Engineering Research and Design* **136**, 610-619. [Crossref]
7. Lijun Wang, Rui Li, Baoxin Wu, Zhenchao Wu, Zhenjun Ding. 2018. Determination of the coefficient of rolling friction of an irregularly shaped maize particle group using physical experiment and simulations. *Particuology* **38**, 185-195. [Crossref]
8. Y. He, T.J. Evans, A.B. Yu, R.Y. Yang. 2018. A GPU-based DEM for modelling large scale powder compaction with wide size distributions. *Powder Technology* **333**, 219-228. [Crossref]
9. Sean Garner, John Strong, Antonios Zavaliangos. 2018. Study of the die compaction of powders to high relative densities using the discrete element method. *Powder Technology* **330**, 357-370. [Crossref]
10. Hyun-Ki Kim, J. Carlos Santamarina. 2018. Spatially Varying Small-strain Stiffness in Soils Subjected to K0 Loading. *KSCE Journal of Civil Engineering* **22**:4, 1101-1108. [Crossref]
11. Y. He, T.J. Evans, Y.S. Shen, A.B. Yu, R.Y. Yang. 2018. Discrete modelling of the compaction of non-spherical particles using a multi-sphere approach. *Minerals Engineering* **117**, 108-116. [Crossref]
12. Kamyar Kildashti, Kejun Dong, Bijan Samali, Qijun Zheng, Aibing Yu. 2018. Evaluation of contact force models for discrete modelling of ellipsoidal particles. *Chemical Engineering Science* **177**, 1-17. [Crossref]
13. Joanna Wiącek, Marek Molenda. 2018. Numerical analysis of compression mechanics of highly polydisperse granular mixtures with different PSD-s. *Granular Matter* **20**:1. . [Crossref]
14. Bereket Yohannes, Marcial Gonzalez, Alberto M. Cuitiño. Discrete Numerical Simulations of the Strength and Microstructure Evolution During Compaction of Layered Granular Solids 123-141. [Crossref]
15. Y. He, T.J. Evans, A.B. Yu, R.Y. Yang. 2017. DEM investigation of the role of friction in mechanical response of powder compact. *Powder Technology* **319**, 183-190. [Crossref]
16. B. Yohannes, M. Gonzalez, A. Abebe, O. Sprockel, F. Nikfar, S. Kiang, A.M. Cuitiño. 2017. Discrete particle modeling and micromechanical characterization of bilayer tablet compaction. *International Journal of Pharmaceutics* **529**:1-2, 597-607. [Crossref]
17. Omid Dorostkar, Robert A. Guyer, Paul A. Johnson, Chris Marone, Jan Carmeliet. 2017. On the role of fluids in stick-slip dynamics of saturated granular fault gouge using a coupled computational fluid dynamics-discrete element approach. *Journal of Geophysical Research: Solid Earth* **122**:5, 3689-3700. [Crossref]

18. Kevin J. Hanley, Catherine O'Sullivan. 2017. Analytical study of the accuracy of discrete element simulations. *International Journal for Numerical Methods in Engineering* **109**:1, 29-51. [Crossref]
19. Yi He, Tim J. Evans, Aibing Yu, Runyu Yang. 2017. Discrete Modelling of Compaction of Non-spherical Particles. *EPJ Web of Conferences* **140**, 01005. [Crossref]
20. Vincent Bürger, Heiko Briesen. 2016. Estimating Colloidal Contact Model Parameters Using Quasi-Static Compression Simulations. *Langmuir* **32**:41, 10784-10794. [Crossref]
21. S. Nadimi, I. Miscovic, J. McLennan. 2016. A 3D peridynamic simulation of hydraulic fracture process in a heterogeneous medium. *Journal of Petroleum Science and Engineering* **145**, 444-452. [Crossref]
22. Joanna Wiącek, Marek Molenda. 2016. Representative elementary volume analysis of polydisperse granular packings using discrete element method. *Particuology* **27**, 88-94. [Crossref]
23. Subhash C. Thakur, Jin Y. Ooi, Hossein Ahmadian. 2016. Scaling of discrete element model parameters for cohesionless and cohesive solid. *Powder Technology* **293**, 130-137. [Crossref]
24. B. Yohannes, M. Gonzalez, A. Abebe, O. Sprockel, F. Nikfar, S. Kiang, A.M. Cuitiño. 2016. Evolution of the microstructure during the process of consolidation and bonding in soft granular solids. *International Journal of Pharmaceutics* **503**:1-2, 68-77. [Crossref]
25. Behrooz Ferdowsi, Michele Griffa, Robert A. Guyer, Paul A. Johnson, Chris Marone, Jan Carmeliet. 2015. Acoustically induced slip in sheared granular layers: Application to dynamic earthquake triggering. *Geophysical Research Letters* **42**:22, 9750-9757. [Crossref]
26. Y. He, Z. Wang, T.J. Evans, A.B. Yu, R.Y. Yang. 2015. DEM study of the mechanical strength of iron ore compacts. *International Journal of Mineral Processing* **142**, 73-81. [Crossref]
27. Junjie Sun, Zhiguo Luo, Zongshu Zou. 2015. Numerical simulation of raceway phenomena in a COREX melter–gasifier. *Powder Technology* **281**, 159-166. [Crossref]
28. Mojtaba Farahnak Langroudi, Abbas Soroush, Piltan Tabatabaie Shourijeh. 2015. A comparison of micromechanical assessments with internal stability/instability criteria for soils. *Powder Technology* **276**, 66-79. [Crossref]
29. Y. He, T.J. Evans, A.B. Yu, R.Y. Yang. 2015. Numerical Modelling of Die and Unconfined Compactions of Wet Particles. *Procedia Engineering* **102**, 1390-1398. [Crossref]
30. Shengqiang Jiang, Tiantian Li, Yuanqiang Tan. 2015. A DEM Methodology for Simulating the Grinding Process of SiC Ceramics. *Procedia Engineering* **102**, 1803-1810. [Crossref]
31. Joanna Wiącek, Marek Molenda. 2014. Effect of particle size distribution on micro- and macromechanical response of granular packings under compression. *International Journal of Solids and Structures* **51**:25-26, 4189-4195. [Crossref]
32. Subhash C. Thakur, John P. Morrissey, Jin Sun, J. F. Chen, Jin Y. Ooi. 2014. Micromechanical analysis of cohesive granular materials using the discrete element method with an adhesive elasto-plastic contact model. *Granular Matter* **16**:3, 383-400. [Crossref]
33. Hao Zhang, Yuanqiang Tan, Shi Shu, Xiaodong Niu, Francesc Xavier Trias, Dongmin Yang, Hao Li, Yong Sheng. 2014. Numerical investigation on the role of discrete element method in combined LBM–IBM–DEM modeling. *Computers & Fluids* **94**, 37-48. [Crossref]
34. Behrooz Ferdowsi, Michele Griffa, Robert A. Guyer, Paul A. Johnson, Chris Marone, Jan Carmeliet. 2014. Three-dimensional discrete element modeling of triggered slip in sheared granular media. *Physical Review E* **89**:4. . [Crossref]

35. Meenakshi Dutt, James A. Elliott. 2014. Granular dynamics simulations of the effect of grain size dispersity on uniaxially compacted powder blends. *Granular Matter* **16**:2, 243-248. [Crossref]
36. Subhash C. Thakur, Hossein Ahmadian, Jin Sun, Jin Y. Ooi. 2014. An experimental and numerical study of packing, compression, and caking behaviour of detergent powders. *Particuology* **12**, 2-12. [Crossref]
37. Erich H. Kisi, Christopher M. Wensrich, Vladimir Luzin, Oliver Kirstein. 2014. Stress Distribution in Iron Powder during Die Compaction. *Materials Science Forum* **777**, 243-248. [Crossref]
38. Mojtaba Farahnak Langroudi, Abbas Soroush, Piltan Tabatabaie Shourijeh, Roozbeh Shafipour. 2013. Stress transmission in internally unstable gap-graded soils using discrete element modeling. *Powder Technology* **247**, 161-171. [Crossref]
39. Xiaoxiong Zha, Chengyong Wan, Yong Fan, Jianqiao Ye. 2013. Discrete element modeling of metal skinned sandwich composite panel subjected to uniform load. *Computational Materials Science* **69**, 73-80. [Crossref]
40. C. M. Wensrich, E. H. Kisi, J. F. Zhang, O. Kirstein. 2012. Measurement and analysis of the stress distribution during die compaction using neutron diffraction. *Granular Matter* **14**:6, 671-680. [Crossref]
41. Kevin J. Hanley, Catherine O'Sullivan, Edmond P. Byrne, Kevin Cronin. 2012. Discrete element modelling of the quasi-static uniaxial compression of individual infant formula agglomerates. *Particuology* **10**:5, 523-531. [Crossref]
42. Ann-Sofie Persson, Göran Frenning. 2012. An experimental evaluation of the accuracy to simulate granule bed compression using the discrete element method. *Powder Technology* **219**, 249-256. [Crossref]
43. Joanna Wiącek, Marek Molenda, Józef Horabik, Jin Y. Ooi. 2012. Influence of grain shape and intergranular friction on material behavior in uniaxial compression: Experimental and DEM modeling. *Powder Technology* **217**, 435-442. [Crossref]
44. Abbas Soroush, Behrooz Ferdowsi. 2011. Three dimensional discrete element modeling of granular media under cyclic constant volume loading: A micromechanical perspective. *Powder Technology* **212**:1, 1-16. [Crossref]
45. Chongbin Zhao. 2011. Computational simulation of frictional drill-bit movement in cemented granular materials. *Finite Elements in Analysis and Design* **47**:8, 877-885. [Crossref]
46. Dongmin Yang, Yong Sheng, Jianqiao Ye, Yuanqiang Tan. 2011. Dynamic simulation of crack initiation and propagation in cross-ply laminates by DEM. *Composites Science and Technology* **71**:11, 1410-1418. [Crossref]
47. Dong Min Yang, Yong Sheng, Jian Qiao Ye, Yuan Qiang Tan, Sheng Qiang Jiang. 2011. Numerical Modelling of Damage Progression in Single-Fiber Composite under Axial Tension. *Advanced Materials Research* **268-270**, 280-285. [Crossref]
48. Simo Matti Siiriä, Osmo Antikainen, Jyrki Heinämäki, Jouko Yliruusi. 2011. 3D Simulation of Internal Tablet Strength During Tableting. *AAPS PharmSciTech* **12**:2, 593-603. [Crossref]
49. Dongmin Yang, Jianqiao Ye, Yuanqiang Tan, Yong Sheng. 2011. Modeling progressive delamination of laminated composites by discrete element method. *Computational Materials Science* **50**:3, 858-864. [Crossref]
50. Yong Sheng, Dongmin Yang, Yuanqiang Tan, Jianqiao Ye. 2010. Microstructure effects on transverse cracking in composite laminae by DEM. *Composites Science and Technology* **70**:14, 2093-2101. [Crossref]
51. Dongmin Yang, Yong Sheng, Jianqiao Ye, Yuanqiang Tan. 2010. Discrete element modeling of the microbond test of fiber reinforced composite. *Computational Materials Science* **49**:2, 253-259. [Crossref]

52. Göran Frenning. 2010. Compression mechanics of granule beds: A combined finite/discrete element study. *Chemical Engineering Science* **65**:8, 2464-2471. [Crossref]

53. Yuan Qiang Tan, Sheng Qiang Jiang, Cai Li, Dong Min Yang, Gao Feng Zhang, Y. Sheng. 2009. Study on Mechanical Properties and Size Effect of Si3N4 Using Discrete Element Method. *Advanced Materials Research* **76-78**, 719-724. [Crossref]

54. Yuanqiang Tan, Dongmin Yang, Yong Sheng. 2009. Discrete element method (DEM) modeling of fracture and damage in the machining process of polycrystalline SiC. *Journal of the European Ceramic Society* **29**:6, 1029-1037. [Crossref]

55. William R. Ketterhagen, Mary T. am Ende, Bruno C. Hancock. 2009. Process Modeling in the Pharmaceutical Industry using the Discrete Element Method. *Journal of Pharmaceutical Sciences* **98**:2, 442-470. [Crossref]

56. A. Mehrotra, B. Chaudhuri, A. Faqih, M.S. Tomassone, F.J. Muzzio. 2009. A modeling approach for understanding effects of powder flow properties on tablet weight variability. *Powder Technology* **188**:3, 295-300. [Crossref]

57. H.P. Zhu, Z.Y. Zhou, R.Y. Yang, A.B. Yu. 2008. Discrete particle simulation of particulate systems: A review of major applications and findings. *Chemical Engineering Science* **63**:23, 5728-5770. [Crossref]

58. C. M. Donahue, C. M. Hrenya, A. P. Zelinskaya, K. J. Nakagawa. 2008. Newton's cradle undone: Experiments and collision models for the normal collision of three solid spheres. *Physics of Fluids* **20**:11, 113301. [Crossref]

59. Xuxin Tu, José E. Andrade. 2008. Criteria for static equilibrium in particulate mechanics computations. *International Journal for Numerical Methods in Engineering* **75**:13, 1581-1606. [Crossref]

60. Göran Frenning. 2008. An efficient finite/discrete element procedure for simulating compression of 3D particle assemblies. *Computer Methods in Applied Mechanics and Engineering* **197**:49-50, 4266-4272. [Crossref]

61. Yuanqiang Tan, Dongmin Yang, Y. Sheng. 2008. Study of polycrystalline Al2O3 machining cracks using discrete element method. *International Journal of Machine Tools and Manufacture* **48**:9, 975-982. [Crossref]

62. Mingjing Jiang, Hai-Sui Yu, Serge Leroueil. 2007. A simple and efficient approach to capturing bonding effect in naturally microstructured sands by discrete element method. *International Journal for Numerical Methods in Engineering* **69**:6, 1158-1193. [Crossref]

63. Chongbin Zhao, T. Nishiyama, A. Murakami. 2006. Numerical modelling of spontaneous crack generation in brittle materials using the particle simulation method. *Engineering Computations* **23**:5, 566-584. [Abstract] [Full Text] [PDF]

64. Frantisek Stepanek, Adeline Loo, Tiong Shing Lim. 2006. Multiscale Modelling Methodology for Virtual Prototyping of Effervescent Tablets. *Journal of Pharmaceutical Sciences* **95**:7, 1614-1625. [Crossref]

65. A.B. Stevens, C.M. Hrenya. 2005. Comparison of soft-sphere models to measurements of collision properties during normal impacts. *Powder Technology* **154**:2-3, 99-109. [Crossref]

66. Yucang Wang, Steffen Abe, Shane Latham, Peter Mora. Implementation of Particle-scale Rotation in the 3-D Lattice Solid Model 1769-1785. [Crossref]